INTERNATIONAL JOURNAL FOR NUMERICAL METHODS IN FLUIDS
Int. J. Numer. Meth. Fluids 2008; **56**:2207–2228
Published online 7 August 2007 in Wiley InterScience (www.interscience.wiley.com). DOI: 10.1002/fld.1581

Numerical analysis of turbulent flow separation in a rectangular duct with a sharp 180-degree turn by algebraic Reynolds stress model

Hitoshi Sugiyama*,†, Tatsuya Tanaka and Hideaki Mukai

Energy and Environmental Science, Graduate School of Engineering, Utsunomiya University, 7-1-2 Yoto, Utsunomiya 321-8585, Japan

SUMMARY

Turbulent flow in a rectangular duct with a sharp 180-degree turn is difficult to predict numerically because the flow behavior is influenced by several types of forces, including centrifugal force, pressure-driven force, and shear stress generated by anisotropic turbulence. In particular, this type of flow is characterized by a large-scale separated flow, and it is difficult to predict the reattachment point of a separated flow. Numerical analysis has been performed for a turbulent flow in a rectangular duct with a sharp 180-degree turn using the algebraic Reynolds stress model. A boundary-fitted coordinate system is introduced as a method for coordinate transformation to set the boundary conditions next to complicated shapes. The calculated results are compared with the experimental data, as measured by a laser-Doppler anemometer, in order to examine the validity of the proposed numerical method and turbulent model. In addition, the possibility of improving the wall function method in the separated flow region is examined by replacing the log-law velocity profile for a smooth wall with that for a rough wall. The analysis results indicated that the proposed algebraic Reynolds stress model can be used to reasonably predict the turbulent flow in a rectangular duct with a sharp 180-degree turn. In particular, the calculated reattachment point of a separated flow, which is difficult to predict in a turbulent flow, agrees well with the experimental results. In addition, the calculation results suggest that the wall function method using the log-law velocity profile for a rough wall over a separated flow region has some potential for improving the prediction accuracy.

Received 4 October 2006; Revised 1 May 2007; Accepted 30 June 2007

KEY WORDS: numerical analysis; turbulent flow; algebraic Reynolds stress model; separated flow; boundary-fitted coordinate system

*Correspondence to: Hitoshi Sugiyama, Energy and Environmental Science, Graduate School of Engineering, Utsunomiya University, 7-1-2 Yoto, Utsunomiya 321-8585, Japan.
†E-mail: sugiyama@cc.utsunomiya-u.ac.jp

1. INTRODUCTION

Flows in ducts are both fundamental and very important because several types of ducts are used, for example, as basic machine elements, in a number of engineering fields. Therefore, several researchers have presented experimental and analytical reports about the flow behavior in ducts in order to contribute to apparatus design. From this point of view, numerical analysis is an effective method to understand flow behavior both in advance and in detail. However, in several cases, ducts have been used for turbulent flows. Compared with laminar flow prediction, the numerical prediction of turbulent flows in ducts is more difficult because the anisotropic turbulent model is needed in order to predict the flow behavior precisely. In addition, abrupt geometrical changes in cross-sections along the flow direction cause flow separation, resulting in the formation of large-scale vortices. The subsequent convection of vortices gives rise to significant flow unsteadiness and has an immediate effect on machine performance. Knowing the separated flow area and the reattachment point in advance leads to improved machine performance. However, in general, a turbulent flow involving separation is one of the most complicated and difficult flows to predict numerically. As such, several studies have examined separated flow both experimentally and analytically [1, 2].

Since flow separation is caused by an abrupt change in the pressure gradient induced by a geometrical change, experimental reports of flow separation are primarily related to diffuser flow and U-bend flow, which have sudden geometrical changes. Buice and Eaton [3] and Obi *et al*. [4] measured in detail the two-dimensional turbulent flows in a one-sided, 10-degree, plane diffuser and reported the mean velocity profile, including the distributions of Reynolds stresses. An expansion ratio of 4.7 was sufficient to produce a separation bubble on a sloping wall. Experiments using U-bend flows are generally classified into two types based on cross-sectional shape. One type is the turbulent flow in a U-bend with a rectangular cross-section, and the other type is the turbulent flow in a U-bend with a circular cross-section. The turbulent separated flow has been measured more often in U-bends with a rectangular cross-section. Hsieh *et al*. [5] measured the two-dimensional turbulent flow in a rotating U-bend with a square cross-section using laser-Doppler anemometry. They presented the main features of the flow and the separated flow, as well as the mean velocity, and the turbulent intensity at particular locations downstream. The measured flow fields are quite complex and consist of secondary cross-stream and radically outward flows due to the Coriolis effects and centrifugal forces. Iacovides *et al*. [6, 7] measured the turbulent flow in a square rotating U-bend typical of coolant passages employed in gas turbine blades using laser-Doppler anemometry. In the upstream and downstream tangents, the pressure and suction surfaces were rough with discrete square cross-sectioned ribs, with a rib pitch-to-height ratio of 10. The introduction of ribs in the straight sections not only reduces the size of the separation bubble along the inner wall of the U-bend by raising the turbulence levels at the bend entry but also causes the formation of an additional separation bubble over the first rib interval along the outer wall, downstream from the bend exit. Recently, Nakayama *et al*. [8] reported in detail the measurement results for a turbulent flow in a rectangular duct with a sharp 180-degree turn, including the distributions of Reynolds stresses. They measured the velocity profiles of the mean velocity in the separated region and the distributions of Reynolds stress, which develop along the stream direction, using laser-Doppler anemometry.

A great number of numerical and experimental measurement results have been reported for a turbulent flow in a duct with separation. Lin *et al*. [9] performed a numerical analysis to study

DOI: 10.1002/fld

the three-dimensional flow and heat transfer in a U-shaped duct of square cross-section under rotating and non-rotating conditions. The computations are based on the ensemble-averaged conservation equations of mass, momentum, and energy. The low Reynolds number shear stress turbulent (SST) model is used in the calculation. Although the calculated results show how the nature of the fluid flow affects the surface heat transfer, there has been no quantitative comparison with the experimental data. Jang *et al.* [10] predicted the three-dimensional flow and heat-transfer for a U-bend with and without 60-degree angled parallel ribs located over the bottom wall of a square cross-section. They reported that the angled rib turbulators over the bottom wall and the 180-degree sharp turn of the channel produced strong non-isotropic turbulence and heat fluxes, which significantly affected the flow fields and heat-transfer coefficients. The calculated distributions of the Nusselt number have been compared with the experimental data, but the profiles of the mean velocity and the Reynolds stress have not been compared with the experimental data. Iacovides and Raisee [11] predicted the turbulent flow and convective heat transfer in passages affected by strong curvature and rib roughness using effective-viscosity and Reynolds stress models. However, they did not compare the Reynolds stress distributions with the experimental data because they examined the prediction of convective heat transfer rather than that of the velocity field. They reported that a low Reynolds differential stress yields more accurate thermal predictions that are superior to those of the low Reynolds effective-viscosity model. Sugiyama and Watanabe [12, 13] calculated the turbulent flow in a U-bend with and without rotation as measured by Iacovides *et al.* [6] by applying the algebraic Reynolds stress model and compared the results with the experimental results, including the distributions of the Reynolds stresses. They reported that the calculated results could reproduce the characteristic features of the experiments.

The above findings suggest that several numerical and experimental analyses have been presented for the turbulent flow under an abrupt change in the pressure gradient induced by a geometrical change, for example, a U-shaped bend or a diffuser. In contrast, few numerical or experimental results have been reported related to turbulent separation, including Reynolds stress. An experimental study was conducted on the flow structure with separation in rectangular channels with a sharp 180-degree turn by Nakayama *et al.* [8]. The mean and fluctuation velocities in three directions, including the separated region, were measured in detail using laser-Doppler anemometry at a Reynolds number of 35 000. They reported that the characteristics of the flow reattachment and the separation bubble inside/after the turn were greatly influenced by the turn clearance, which was defined as the distance between the inner and outer walls in the bend region. These experimental results are also useful for evaluating the validity of turbulent models.

Based on the above-mentioned studies, the main purpose of the present thesis is to predict numerically the turbulent flow in a rectangular channel with a sharp turn, as reported by Nakayama *et al.* [8], in order to estimate the validity of an algebraic Reynolds stress model. In addition, the wall function method, which is used to set the boundary conditions for the turbulent energy and dissipation, is examined. The generation of separated flow acts on the duct as flow resistance, which suggests that the separated region acts as a kind of rough wall. More concretely, the log-law velocity profile for a rough wall is applied only to the separated region rather than that generally used for a smooth wall. The calculated results quantitatively show the difference in prediction accuracy between these two types of log-law velocity.

DOI: 10.1002/fld

2. MATHEMATICAL FORMULATION

2.1. Numerical object and definition of the coordinate system

Figure 1 shows schematic diagrams of rectangular channels with sharp 180-degree turns that are selected as numerical objects in this calculation. Nakayama *et al*. [8] measured the turbulent flow including a separated flow in these channels in detail, using a laser-Doppler anemometer. They presented three types of experimental data that were measured for varying channel width, which is defined as the distance between the outer and the inner walls at a sharp turning duct, i.e. 30, 50, and 70 mm. Note that the channel width changes only in sharp turn sections. The experimental flume with a rectangular cross-section has a width of 50 mm, a depth of 25 mm, and a length of 334 mm, as shown in Figure 1. The Reynolds number is 3.5×10^4 based on hydraulic diameter and bulk velocity. In this calculation, the channel width in the sharp turn section is 50 mm.

The coordinate systems used in the calculation are also defined in Figure 1. In the rectangular channel, the main flow direction is represented by the X_1-axis except for a straight channel with a sharp turn, and the secondary flow directions are denoted by the X_2- and X_3-axes, which represent the horizontal and vertical directions, respectively. The origin of the rectangular coordinate system is set at the central point of the inner wall located on the inlet cross-section of the main straight channel.

2.2. Governing transport equations

The transport equation of momentum is expressed in the following form through the ensemble-averaged operation and is indispensable in solving the Reynolds stresses appearing in the transport equation in order to completely obtain the velocity fields

$$\frac{\mathrm{D}\overline{U_i}}{\mathrm{D}t} = -\frac{1}{\rho}\frac{\partial \overline{P}}{\partial X_i} + \frac{\partial}{\partial X_j}\left(\nu \frac{\partial \overline{U_i}}{\partial X_j} - \overline{u_i u_j}\right) \tag{1}$$

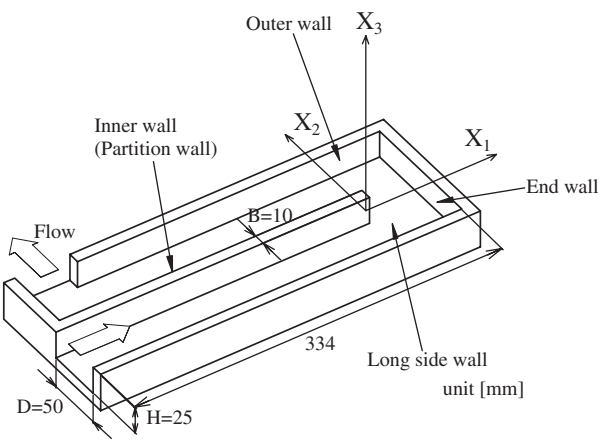

Figure 1. Schematic diagram of the experimental apparatus and the definition of the coordinate system.

DOI: 10.1002/fld

Table I. Modeling of the pressure–strain correlation term.

$\pi_{ij,1}+\pi_{ji,1}$	$-C_1\frac{\varepsilon}{k}\left(\overline{u_iu_j}-\frac{2}{3}k\delta_{ij}\right)$
$\pi_{ij,2}+\pi_{ji,2}$	$-\frac{C_2+8}{11}\left(P_{ij}-\frac{2}{3}P_k\delta_{ij}\right)+\zeta k\left(\frac{\partial U_i}{\partial x_j}+\frac{\partial U_j}{\partial x_i}\right)-\frac{8C_2-2}{11}\left(D_{ij}-\frac{2}{3}P_k\delta_{ij}\right)$
$[\pi_{ij}+\pi_{ji}]_{\mathrm{w}}$	$C_1=C_1^*+C_1'f\left(\frac{L}{X_{\mathrm{w}}}\right),\quad C_2=C_2^*+C_2'f\left(\frac{L}{X_{\mathrm{w}}}\right),\quad \zeta=\zeta^*+\zeta'f\left(\frac{L}{X_{\mathrm{w}}}\right)$
	$P_{ij}=-\overline{u_iu_k}\frac{\partial U_i}{\partial x_k}-\overline{u_ju_k}\frac{\partial U_i}{\partial x_k},\quad D_{ij}=-\overline{u_iu_k}\frac{\partial U_k}{\partial x_j}-\overline{u_ju_k}\frac{\partial U_k}{\partial x_i}$
	$P_k=-\overline{u_ku_l}\frac{\partial U_k}{\partial x_1},\quad f\left(\frac{L}{X_{\mathrm{w}}}\right)=\frac{C_\mu^{3/4}}{\kappa}\frac{k^{3/2}}{\varepsilon}\frac{1}{X_{\mathrm{w}}}$

In this calculation, we have adopted the transport equation of Reynolds stresses to predict anisotropic turbulence accurately. The transport equation of Reynolds stresses is displayed exactly in the following form:

$$\frac{\mathrm{D}\overline{u_iu_j}}{\mathrm{D}t}=-\left(\overline{u_iu_k}\frac{\partial U_j}{\partial X_k}+\overline{u_ju_k}\frac{\partial U_i}{\partial X_k}\right)+\overline{\frac{p}{\rho}\left(\frac{\partial u_i}{\partial X_j}+\frac{\partial u_j}{\partial X_i}\right)}$$
$$-\frac{\partial}{\partial X_k}\left\{\overline{u_iu_ju_k}-\nu\frac{\partial\overline{u_iu_j}}{\partial X_k}+\overline{\frac{p}{\rho}(\delta_{jk}u_i+\delta_{ik}u_j)}\right\}-2\nu\overline{\frac{\partial u_i}{\partial X_k}\frac{\partial u_j}{\partial X_k}} \tag{2}$$

It is impossible to numerically solve the above equation directly, so it is necessary to rewrite several terms of the Reynolds stress equation by introducing the concept of the turbulent model. Moreover, in numerical analysis, the convection term on the left-hand side and the diffusion term on the right-hand side are obstacles in obtaining a numerical solution because these terms are required in order to carry out iterative calculations to obtain stable results. In the present study, these terms are modeled by adopting Rodi's [14] approximation. As a result of this approximation, these two terms are transformed into an algebraic form rather than a differencing form. Therefore, the convection and diffusion terms in the above equation were modeled as follows:

$$\frac{\mathrm{D}\overline{u_iu_j}}{\mathrm{D}t}-\mathrm{Diff}_{ij}=\frac{\overline{u_iu_j}}{2k}(P_k-\varepsilon) \tag{3}$$

where Diff_{ij} corresponds to the third term on the right-hand side of Equation (2) and P_k represents the production term of the turbulent energy equation.

A particularly problematic task here is the modeling of the pressure–strain correlation equation term, which is also defined as the redistribution term and is shown as the second term on the right-hand side of Equation (2). The pressure–strain term is composed of three parts, which are the interaction of the fluctuating velocities ($\pi_{ij,1}+\pi_{ji,1}$), the interaction of the mean strain with the fluctuating velocities ($\pi_{ij,2}+\pi_{ji,2}$), and the wall proximity effects ($\pi_{ij,w}+\pi_{ji,w}$). In the present calculation, we have adopted Rotta's linear return to isotropy mode for the ($\pi_{ij,1}+\pi_{ji,1}$) term, as shown in Table I.

For $\pi_{ij,2}$, the correlation is approximated as

$$\pi_{ij,2}=\left(\frac{\partial U_l}{\partial X_m}\right)a_{lj}^{mi} \tag{4}$$

DOI: 10.1002/fld

Table II. Model constants of the pressure–strain correlation term.

C_1^*	C_2^*	ζ^*	C_1'	C_2'	ζ'	C_μ	κ
1.4	0.44	−0.16	−0.35	0.12	−0.1	0.09	0.42

and a_{lj}^{mi} is the fourth-order tensor, which should satisfy the following kinematic constraints:

$$a_{lj}^{mi} = a_{lj}^{im} = a_{jl}^{im} \tag{5}$$

$$a_{lj}^{mi} \frac{\partial U_l}{\partial X_m} = 0 \tag{6}$$

$$a_{jj}^{mi} = 2\overline{u_m u_i} \tag{7}$$

The above constraints arise from the symmetry condition, the mass conservation law, and Green's theorem, respectively. Although the kinematic constraint of Equation (6) is different from that reported by Launder *et al.* [15], we adopted Equation (6) because $\pi_{ij,2}$ is defined as the production between the fourth-order tensor and the mean strain, as shown in Equation (4). Gessner and Eppich [16] have also reported these constraints and described them in detail. In terms of the modeling of $(\pi_{ij,2} + \pi_{ji,2})$, the modeling process is described in detail in a previous report by Sugiyama and Hitomi [17]. In addition, the validity of the presented model has been confirmed by the calculation carried out for a turbulent flow in a meandering open-channel flow [18]. In the case of calculation in open-channel flow, the boundary condition along the free surface and the turbulent model are important factors to precisely predict open-channel flow because anisotropic turbulence is produced near the free surface. A method for establishing the boundary condition along the free surface has been presented, along with the modeling of the pressure–stain term, in Reference [18]. The interaction of mean strain with fluctuating velocities $(\pi_{ij,2} + \pi_{ji,2})$ is finally modeled as shown in Table I.

The wall effect term $(\pi_{ij,w} + \pi_{ji,w})$ on turbulent stresses is modeled as shown in Table I by changing the model constants. In Table I, $f(L/X_w)$ is a function related to the dimensionless distance from the wall, and c_μ and κ represent the empirical constant and the von Karman constant, respectively. The function $f(L/X_w)$ is that of a unit value near the wall, which approaches zero with increasing distance from the wall. The symbol X_w is the normal distance from the wall, and L defines the length scale of turbulence. When $f(L/X_w)$ is zero, the model yields the correct Reynolds stress components for the nearly homogeneous share flow of Champangne *et al*. [19]. In contrast, when $f(L/X_w)$ is of unit value, the magnitude of the stress components agrees with the consensus of the near wall turbulence. The model constants used in this analysis are summarized in Table II.

The fourth term on the right-hand side of Equation (2) is the homogeneous part of dissipation. The dissipation rate everywhere in the computed flow was assumed to be locally isotropic, i.e.

$$\varepsilon_{ij} = 2\nu \overline{\frac{\partial u_i}{\partial X_k} \frac{\partial u_j}{\partial X_k}} = \frac{2}{3}\delta_{ij}\varepsilon \tag{8}$$

DOI: 10.1002/fld

The transport equations of turbulent energy and dissipation are expressed in the following form:

$$\frac{\mathrm{D}k}{\mathrm{D}t} = \frac{\partial}{\partial X_j}\left\{\left(\nu\delta_{jk} + c_\mathrm{s}\frac{k}{\varepsilon}\overline{u_k u_j}\right)\frac{\partial k}{\partial X_k}\right\} - \overline{u_i u_k}\frac{\partial U_i}{\partial X_k} - \varepsilon \tag{9}$$

$$\frac{\mathrm{D}\varepsilon}{\mathrm{D}t} = \frac{\partial}{\partial X_j}\left\{\left(\nu\delta_{jk} + c_\varepsilon\frac{k}{\varepsilon}\overline{u_k u_j}\right)\frac{\partial \varepsilon}{\partial X_k}\right\} - \frac{\varepsilon}{k}\left(c_{1\varepsilon}\overline{u_i u_k}\frac{\partial U_i}{\partial X_k} + c_{2\varepsilon}\varepsilon\right) \tag{10}$$

Model constants c_s, c_ε, $c_{1\varepsilon}$, and $c_{2\varepsilon}$ are 0.22, 0.18, 1.44, and 1.92, respectively.

3. NUMERICAL ASPECTS

3.1. Boundary-fitted coordinate system

For calculation, the boundary condition must be set precisely next to the complicated shape. In this calculation, a boundary-fitted coordinate system, which is a type of coordinate transformation method, is introduced. The coordinate in the physical plane can be transformed to that in the calculation plane using the boundary-fitted coordinate system. Numerical calculation is performed in the calculation plane because setting the boundary conditions next to the complicated shape is easy. In addition, note that the governing equations are transformed into complicated equations from simple equations that are expressed in the physical plane, although it is easy to set boundary conditions next to the complicated shape.

The transformation from the physical plane to the calculation plane is performed by using the following mathematical theorem:

$$\frac{\partial}{\partial X_i} = \frac{\partial \xi}{\partial X_i}\frac{\partial}{\partial \xi} + \frac{\partial \eta}{\partial X_i}\frac{\partial}{\partial \eta} + \frac{\partial \zeta}{\partial X_i}\frac{\partial}{\partial \zeta} \tag{11}$$

where ξ, ζ and η represent the coordinates of the calculation plane and correspond to the main flow and the cross-sectional directions along the computational grid.

3.2. Examination of wall function method

In the proposed turbulent model, the wall function method is used to set the boundary conditions for turbulent energy and dissipation. Adopting the wall function method along the walls, it is necessary to obtain the values of turbulent energy and dissipation in order to assume the log-law velocity profile over the walls. The following log-law velocity profile for a smooth wall is assumed for several numerical analyses:

$$\frac{U_1}{U_\tau} = \frac{1}{0.42}\ln\left(\frac{U_\tau y}{\nu}\right) + 5.5 \tag{12}$$

The above equation may not be applicable to the separated flow region. The separated flow is thought of as a flow resistance in channel flow because the separated flow generates a great pressure loss in the channel. Thus, it is assumed that the log-law velocity profile for a rough wall is used only for a region covered by a separated flow. In the calculation, although the log-law velocity profile can be freely assumed for a rough wall, the following log-law velocity profile, as measured by Fujita *et al*. [20], is introduced because they systematically measured the turbulent

DOI: 10.1002/fld

flow in a rectangular duct with rough walls and quantitatively reported the flow situation and the configuration of the rough wall:

$$\frac{U_1}{U_\tau} = \frac{1}{0.42} \ln\left(\frac{U_\tau y}{\nu}\right) - 8.62 \tag{13}$$

The numerical analysis of turbulent flow in a square duct with one roughened wall has been carried out to confirm the validity of the log-law velocity (13) and the presented turbulent model in both velocity and temperature fields [21]. As a result of this analysis, the proposed turbulent model could reproduce the secondary flow of the second type, which has been reported to be a typical phenomenon induced by anisotropic turbulence using the above log-law velocity.

In this simulation, two types of calculations are carried out in order to examine the effect of the log-law velocity profile for a rough wall applied to the separated flow region rather than that for a smooth wall. First, the turbulent flow is calculated over all the walls using the log-law velocity profile for a smooth wall. Second, the turbulent flow is predicted by adopting the log-law velocity profile for a rough wall over the separated flow region only.

3.3. Numerical analysis

Figure 2 shows two types of computational grids. The upper grid is a top view of a duct with a sharp turn, and the lower grid is the sectional grid layout for a rectangular duct. The inlet length of the rectangular duct is the same as that of the experimental apparatus, and an outlet length of 30 times the hydraulic diameter is set downstream from the end wall in order to make use of the free-stream condition at the outlet section in the numerical analysis. The initial values of turbulent energy and dissipation were assumed to be $k = U_b^2 \times 10^{-5}$ and $\varepsilon = k^{3/2}/D$, respectively. Since the proposed turbulent model can be classified as a high Reynolds-number turbulent model, the wall function method is adopted as the boundary condition for the turbulent energy and dissipation at

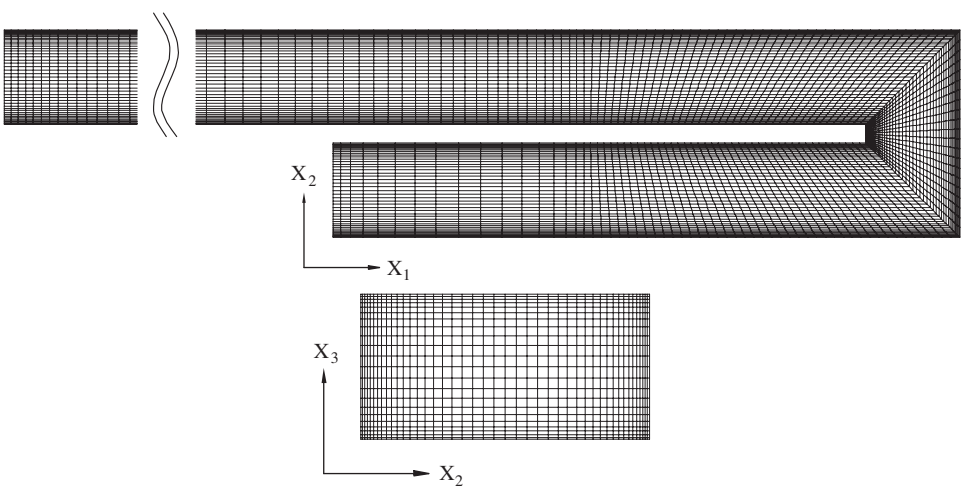

Figure 2. Computational grid layout.

DOI: 10.1002/fld

the first grid point from the wall. Fine grids are used near the wall because the physical parameters change rapidly near the wall. Although it is necessary to examine the grid dependency, the grid layout in Figure 2 has been adopted for this analysis because the presented method is able to predict correctly the reattachment point of the separation flow, which is described in the following section. The governing equations were discretized by the differencing scheme, and QUICK (a third-order up-wind differencing scheme) was used for the convection term. Based on the hydraulic radius and the bulk velocity, the Reynolds number is 3.5×10^4. The total cross-section has a total of 45×23 computational grid points, and 218 grid points are set along the main flow direction. Therefore, the total number of computational grids is 225 630.

4. RESULTS AND DISCUSSIONS

The experimental results were measured in detail on both the X_1–X_2 plane and on cross-sections along the flow direction. Figure 3 shows the measurement sections, which are denoted as Sections 1–6. The calculated results are compared quantitatively with the experimental results obtained for Sections 1–6. In the present study, two types of calculations are performed in order to examine the validity of using the wall function method for a rough wall over a separated region. The first calculation is the prediction of the channel flow using the log-law velocity profile under the assumption that all the walls are smooth. In the second calculation, the log-law velocity profile is adopted for a rough wall covering only the separated region. Using the universal constant of the log-law velocity, for the first calculation we assume that $C = 5.5$, and for the second calculation we assume that $C = -8.62$.

4.1. Comparison of mean velocity

The results calculated for the main flow velocities are compared with the experimental data at the six stations, as shown in Figure 4. The results for each section are arranged in order from the top (i.e. the experimental results, the calculated results for $C = -8.62$, and the calculated results for $C = 5.5$). The calculated and experimentally obtained results are both normalized by

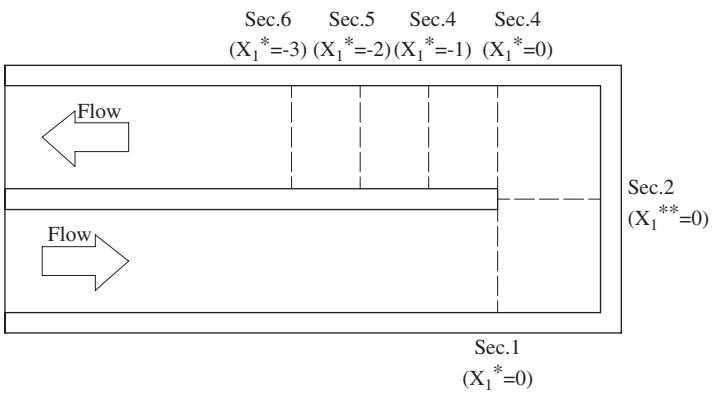

Figure 3. Locations of cross-sections used in the calculation and in the experiment.

DOI: 10.1002/fld

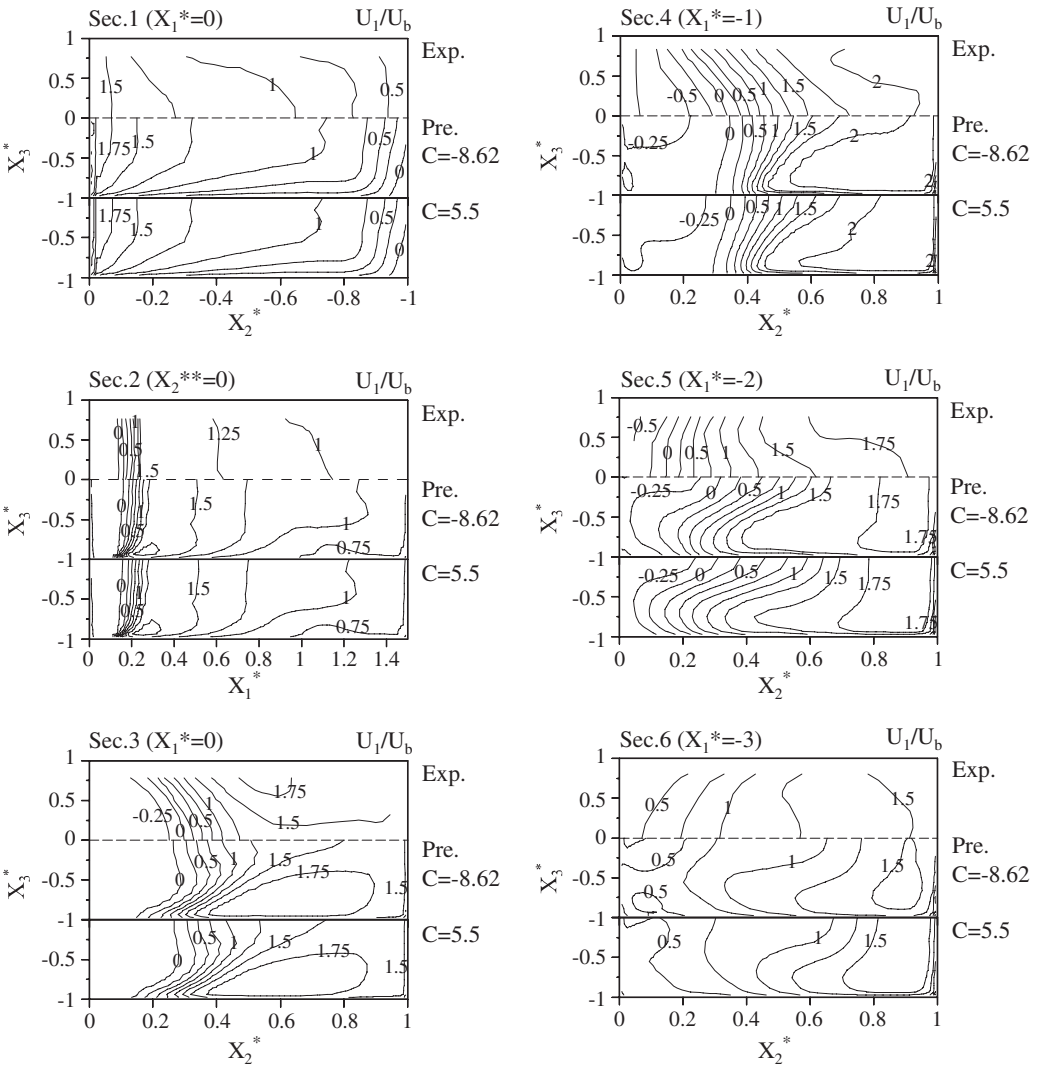

Figure 4. Comparison of main flow velocity.

the bulk mean velocity. The notations $X_2^* = 0$ and 1 indicate the inner and outer walls of the duct, respectively. Section 1 is located in the inlet cross-section of the curved duct. A characteristic feature of the curved duct with a circular cross-section is that the maximum stream-wise velocity is located on the inner wall side in the circular cross-section. This feature is typical of curved ducts and is confirmed for this rectangular duct, as shown in the inlet cross-section of Section 1. The zero-valued contour lines differed for the experimental and calculated results, i.e. the calculation predicted that the contour line would lie near the outer wall. The experimental results for the contour lines of Section 2, which represent the middle of the curved duct, indicate the existence of a separated flow near the inner wall. The calculation also correctly predicts the location of the

DOI: 10.1002/fld

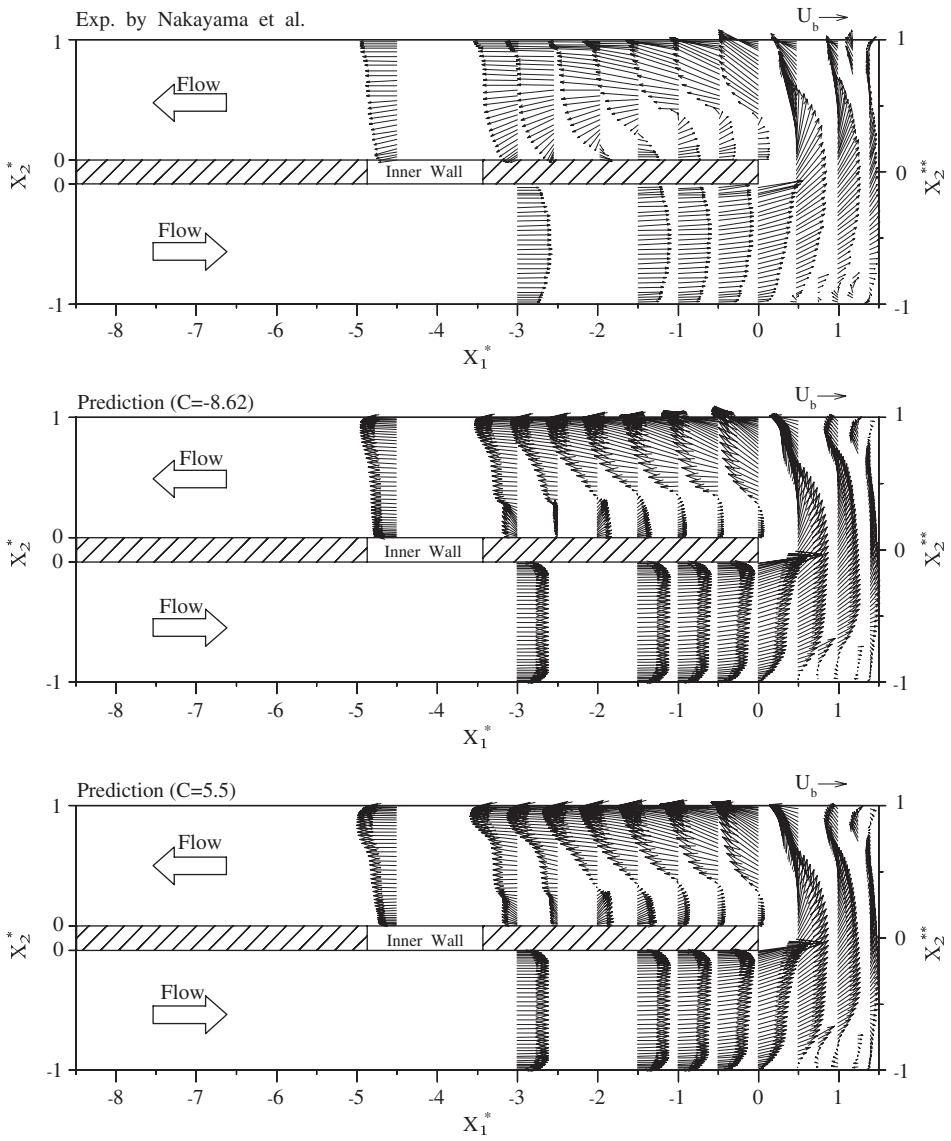

Figure 5. Comparison of stream-wise velocity vectors in the X_1–X_2 plane.

zero-valued contour line. The cross-sections of Sections 3–5 are located only in the separated flow generated in the straight duct following the curved duct with a sharp turn. When the location of the zero-valued contour line is considered, the calculation correctly reproduces the experimental contour lines, except those of Section 5. For Section 5, the experimentally obtained zero-valued contour line is located near the inner wall, whereas the calculated contour line is located far from the inner wall. In addition, the calculated contour lines are distorted near the lower wall, whereas

DOI: 10.1002/fld

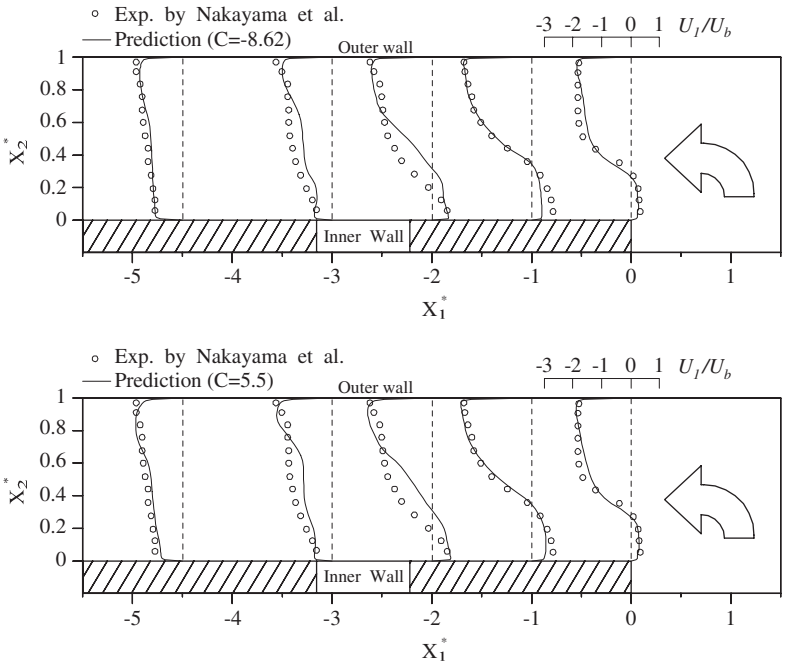

Figure 6. Comparison of stream-wise velocity along the X_2-axis.

the experimentally obtained contour lines are not. These distorted contour lines are formed more clearly for Sections 5 and 6, which are located downstream from the separated region.

Figure 5 compares the results for the stream-wise velocity vectors in the X_1–X_2 plane. In both the experimental and calculated results, large-scale and small-scale separations are observed in the downstream straight duct and in the corner regions of the curved duct with a sharp turn, respectively. Although separated flows are recognized in both the experimental and calculated results, the calculated velocity profiles in the separated region differ slightly from the experimental values. The local stream-wise velocity and the velocity in the X_2 direction are compared quantitatively with the experimentally obtained values in order to evaluate in detail the validity of the proposed calculation. Figures 6 and 7 compare the results for the stream-wise velocity and the velocity in the X_2 direction, respectively. These figures suggest that the difference between the experimental and the calculated results of the velocity profiles along the X_2 direction is more significant than that for the stream-wise velocity. In particular, the velocity profiles at $X_1^* = -2$ and -1, which are located near the reattachment point of the separated flow, are in the opposite direction compared with the experiment values near the inner wall.

For the turbulent model, a precise prediction of the reattachment point of the separated flow is important. Therefore, the distribution of the stream function is compared with the experimental results for the velocity field. Generally, the stream function is used for two-dimensional flows, but the distribution of the stream function is introduced in the experiment in order to clarify the reattachment point of the separated flow. Therefore, the calculated distribution of the stream function is compared with the experimentally obtained distribution. Figure 8 compares the results of the stream function in the X_1–X_2 plane. The two methods proposed for the log-law velocity

DOI: 10.1002/fld

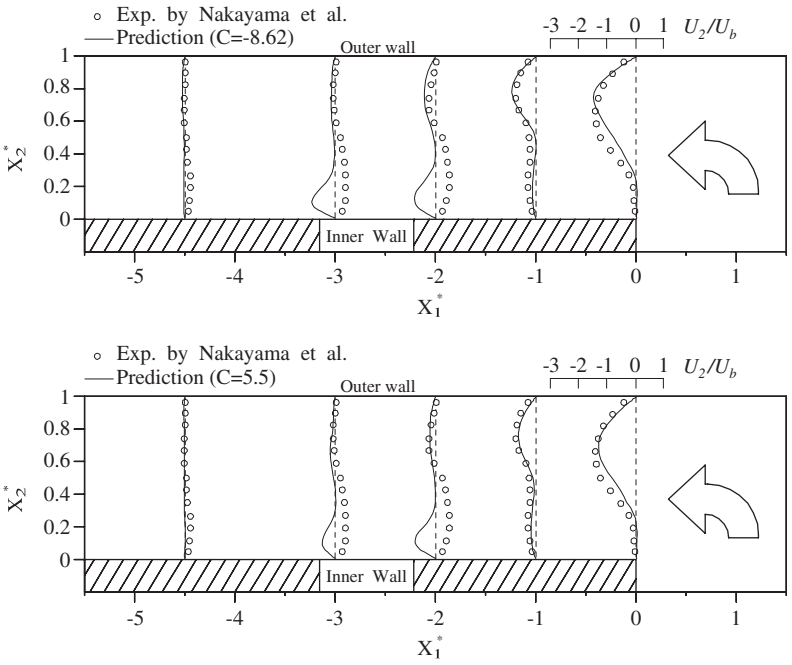

Figure 7. Comparison of horizontal velocity along the X_2-axis.

profile predict the reattachment point well with no great discrepancy. When the contour line for 0.15 of the experiment is considered, the calculated results for $C = -8.62$ are closer to the experimental results than those for $C = 5.5$. The method using the log-law velocity profile for a smooth wall tends to overestimate the value for 0.15, which implies that this method has some potential for improving the prediction accuracy by changing the value of the universal constant C of the log-law velocity.

The vector plots of Figure 9 present a comparison of the secondary flow for cross-sections of the stream-wise flow. The calculated rotating direction shows the opposite direction of the experiment because symmetrical cross-sections with respect to X_2-axis are compared. In Section 1, the calculation predicts the secondary flow to move uniformly from the outer wall to the inner wall as is the case of the experimental results. This secondary flow behavior for a curved duct with a circular cross-section has been reported to be caused by the pressure imbalance between the low pressure of the inner wall side and the high pressure of the outer wall side. The experimental measurement of Section 2 shows the generation of the circulation flow along the upper wall, which is formed by the secondary flow. Although the proposed methods also reproduce this circulating flow, the region covered by the circulated flow is larger and clearer than in the experiment.

The cross-sections of Sections 3–5 are located only in the separated flow generated in the straight duct following the curved duct with a sharp turn. The experimental results for Sections 3 and 4 indicate that the secondary flow located in the separated region has a low velocity on the inner wall side, and, in contrast, except for the separated region, the secondary flow has a high value for the circulation flow. The calculated results also reproduce these characteristic features. Comparing the calculated results for $C = -8.62$ and 5.5, the calculated region for $C = -8.62$ covered by a

DOI: 10.1002/fld

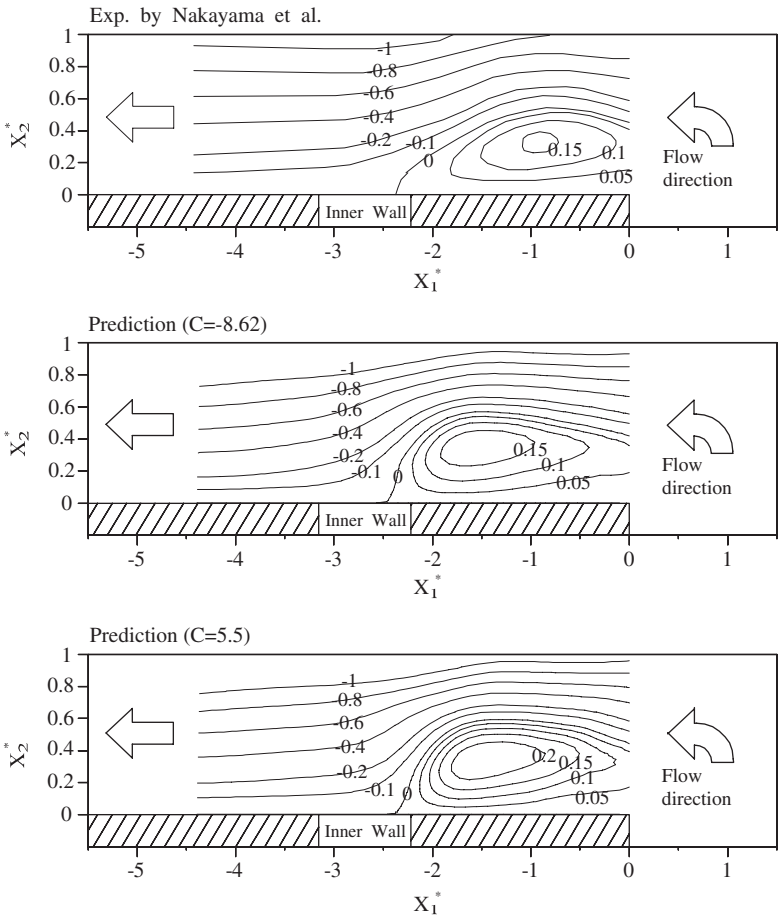

Figure 8. Comparison of stream function over the separated flow in the X_1–X_2 plane.

low-velocity flow is slightly larger than that in the case of $C = 5.5$. This difference is caused by applying a different log-law velocity to the separated region. In Section 5, which is located near the reattachment point, both calculations predict well a pair of vortices on the inner wall side, while no vortex was observed in the experimental results. In contrast, a large circulation flow on the outer wall side is observed for both the experimental and calculated results.

The flow conditions in Section 6 correspond to the downstream flow from the reattachment point. The circulation flow generated in the previous section gradually decays as the flow develops, as shown in Section 6. The calculated results show that a pair of vortices on the inner wall side in Section 5 maintains the flow pattern of circulation even if the intensity decreases as the flow develops. Recently, Nakayama *et al.* [22] measured a turbulent flow in the same cross-section with a sharp 180-degree turn using particle image velocimetry (PIV). Although the Reynolds number (2.0×10^4) and the location of the measurement section are not identical to those of the present study, a pair of vortices clearly appears on the inner wall side. This agreement indicates the validity of the proposed method of calculation.

DOI: 10.1002/fld

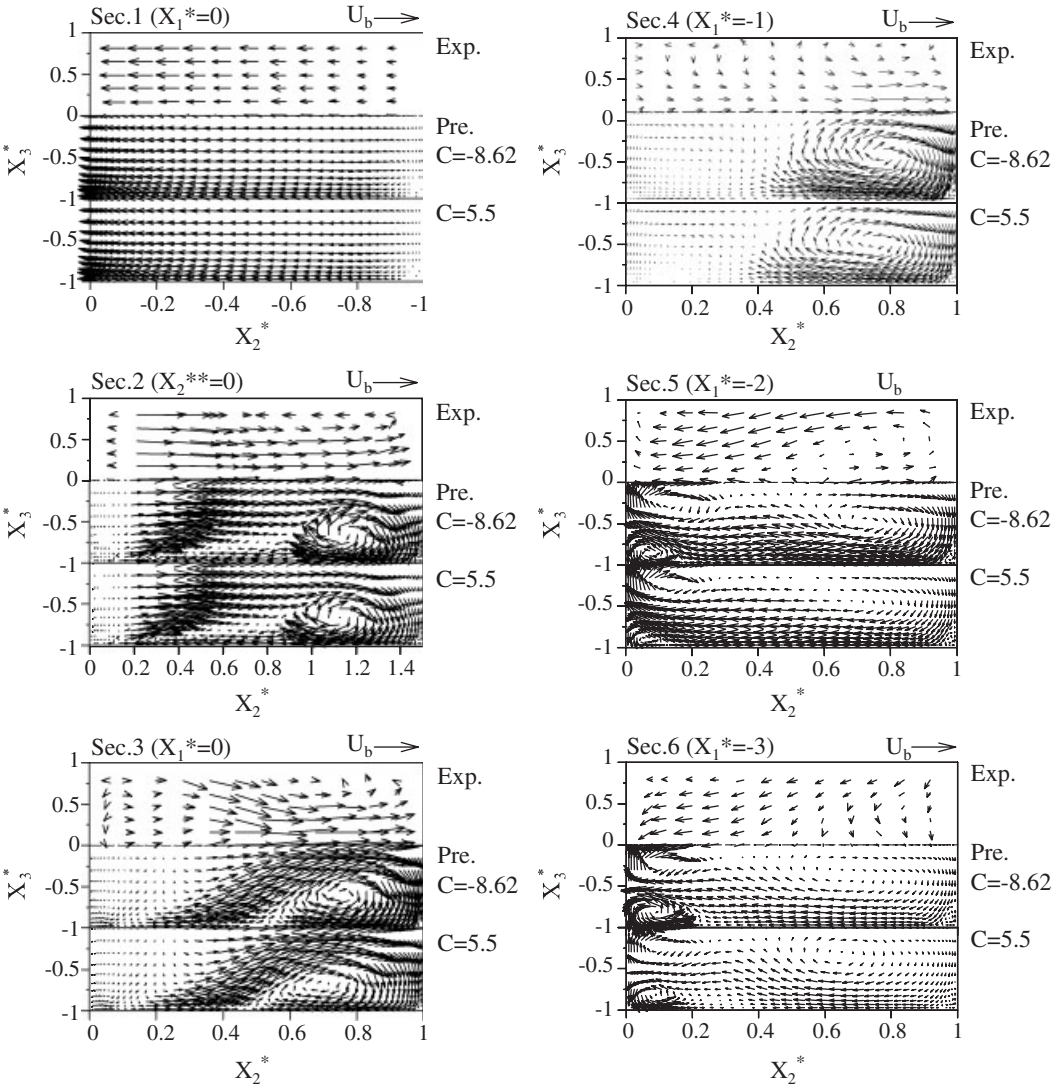

Figure 9. Cross-sectional comparison of the secondary flow vectors.

4.2. Comparison of distributions of fluctuating velocity

Figure 10 compares turbulent energy distributions. The calculated contour lines are normalized by the average mean velocity, as are the experimental results. Comparing the results for the turbulent energy reveals that the calculated results for Sections 4–6 are in relatively good agreement with the experimental results, whereas the results calculated for Sections 1–3 have a different distribution from the experimental results. In particular, the calculation predicts contour lines with a high value near the bottom wall of the outer wall side, as shown in the compared result of Section 2. In addition, comparison of the results for Section 3 indicates that the maximum calculated value is

DOI: 10.1002/fld

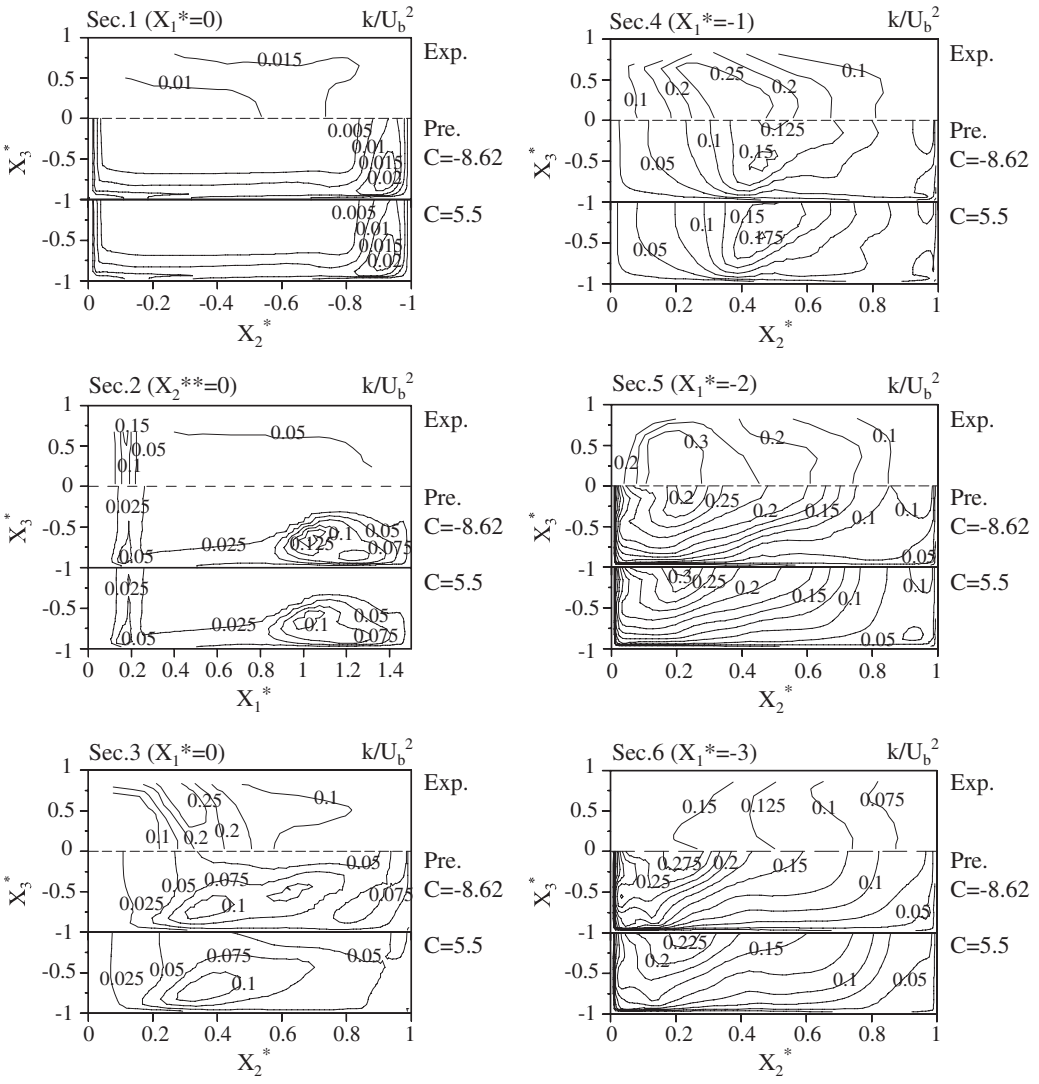

Figure 10. Comparison of turbulent energy.

lower than the maximum experimental value, although the calculated and experimental locations for the maximum value are in approximate agreement.

Figure 11 shows the comparison of the main flow fluctuating velocity, which forms a part of the turbulent energy. For Section 1, the calculated and experimental maximum values are generated near the outer wall. Further downstream, in Section 2, the experimental maximum value (0.4) appears on the inner wall side. This coincides with the location of the shear layer generated by the separated flow. Based on the fact that the calculation cannot correctly reproduce the maximum value but instead predicts a relatively high value near the inner wall side, the calculation tends to predict a lower value than that obtained in the experiment.

DOI: 10.1002/fld

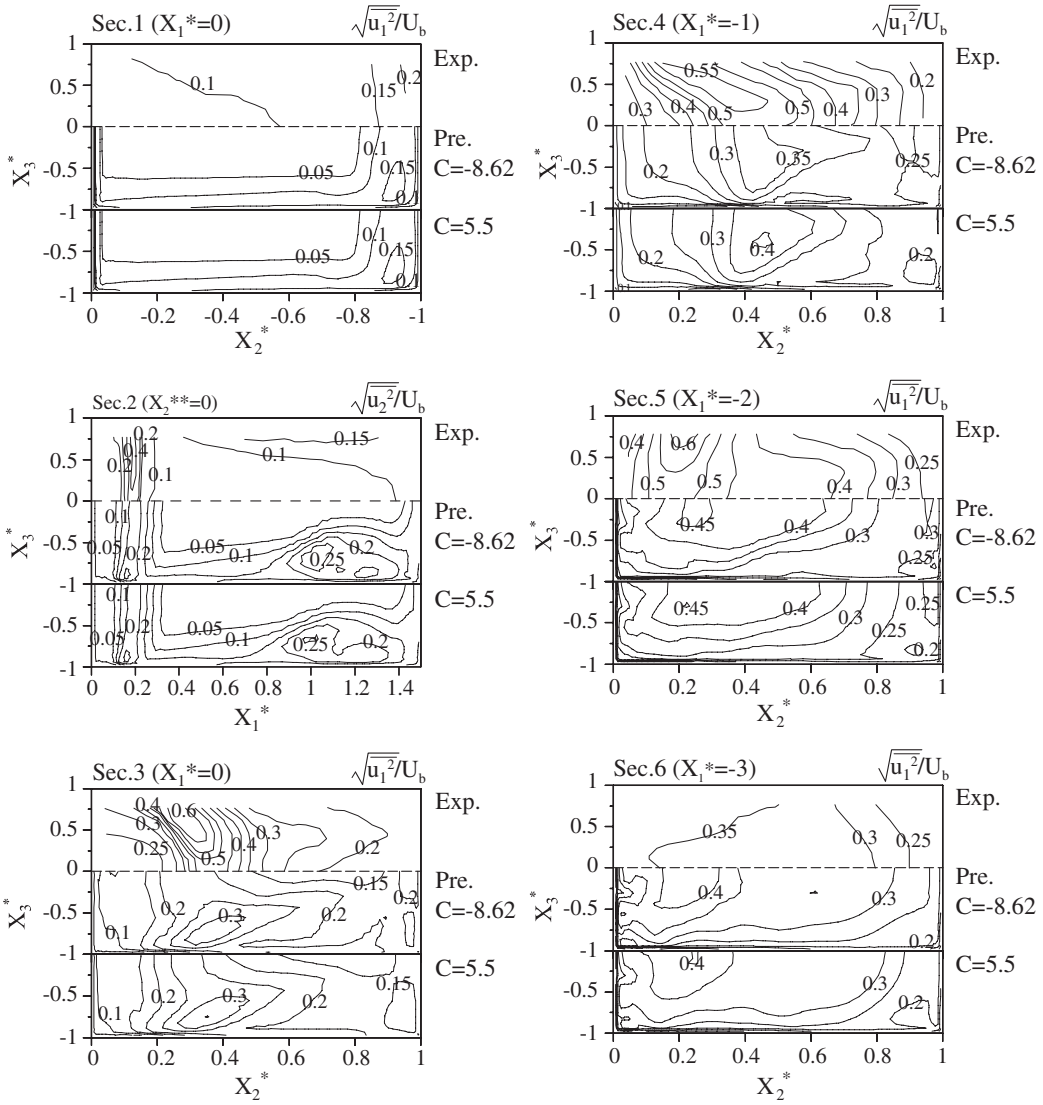

Figure 11. Comparison of the stream-wise fluctuating velocity.

The experimental results for Sections 3–5, which are located in the separated flow, show that the maximum value is generated near $X_2^* = 0.2$ of the upper wall in all cross-sections. The calculated results for Section 3 show the same tendency as well. However, except for Section 3, the maximum values occur in the central region of the cross-sections; this feature differs from the experimental feature. In Section 6, which is located after the reattachment point, the maximum value is produced near the inner wall for both results, although for the experiment, there are no contour lines near the inner wall.

DOI: 10.1002/fld

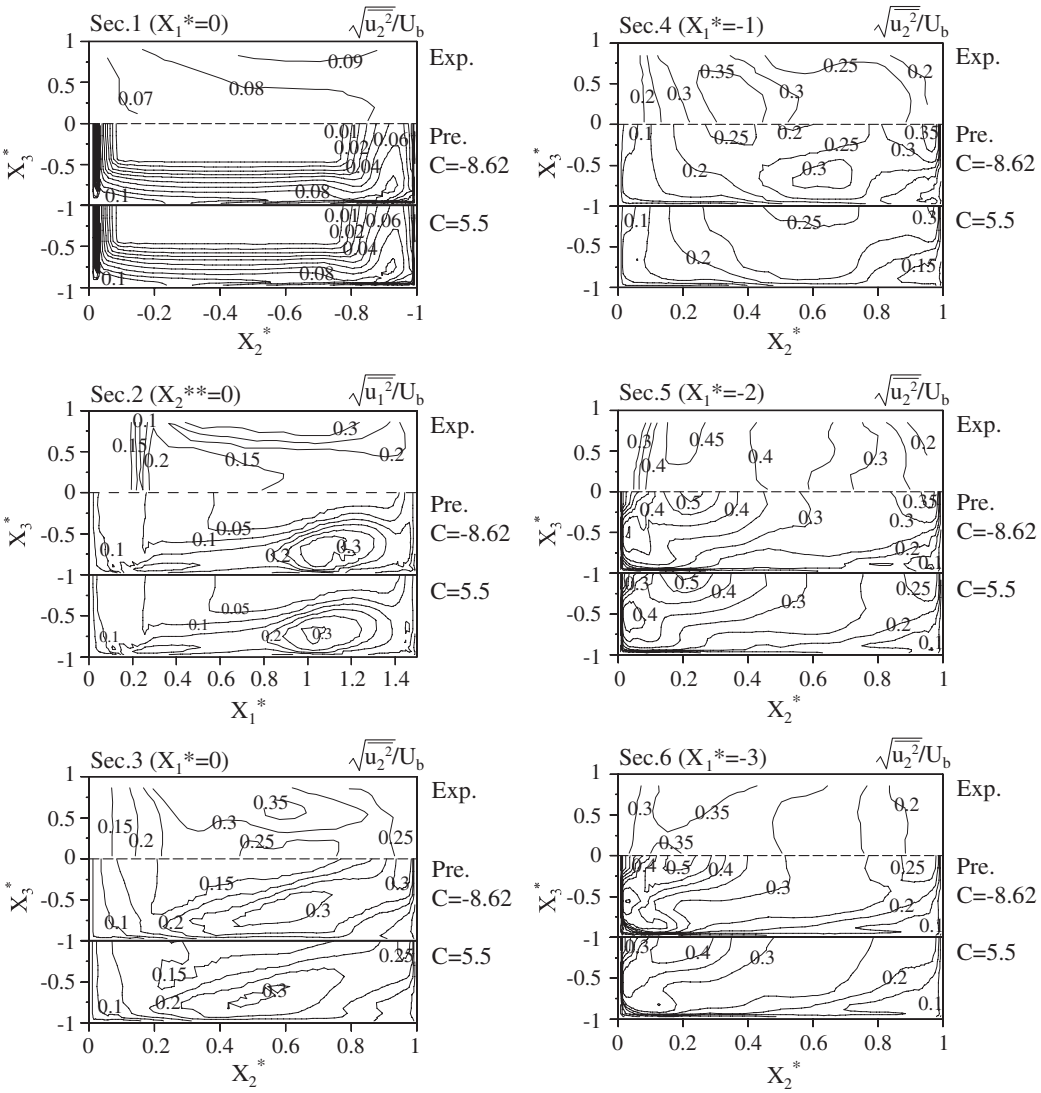

Figure 12. Comparison of horizontally fluctuating velocity.

Figure 12 compares the fluctuating velocity in horizontal direction parallel to the X_2^*-axis. Both the experimental and calculated results for Section 1 have the maximum value along the X_2^*-axis. In addition, in the experiment, for Sections 3–5, high values are generated for the fluctuating velocity in the region ranging from the long side wall to the central region of the rectangular cross-section. The calculation can also reproduce this experimental feature, although the agreement with the experimental value is not perfect. The generation term of the fluctuating velocity in the horizontal direction is composed of velocity gradients, i.e. $\partial U_2/\partial X_1$, $\partial U_2/\partial X_2$, and $\partial U_2/\partial X_3$. Therefore, in the case of a straight duct, the maximum value is generated near the wall because of the velocity

DOI: 10.1002/fld

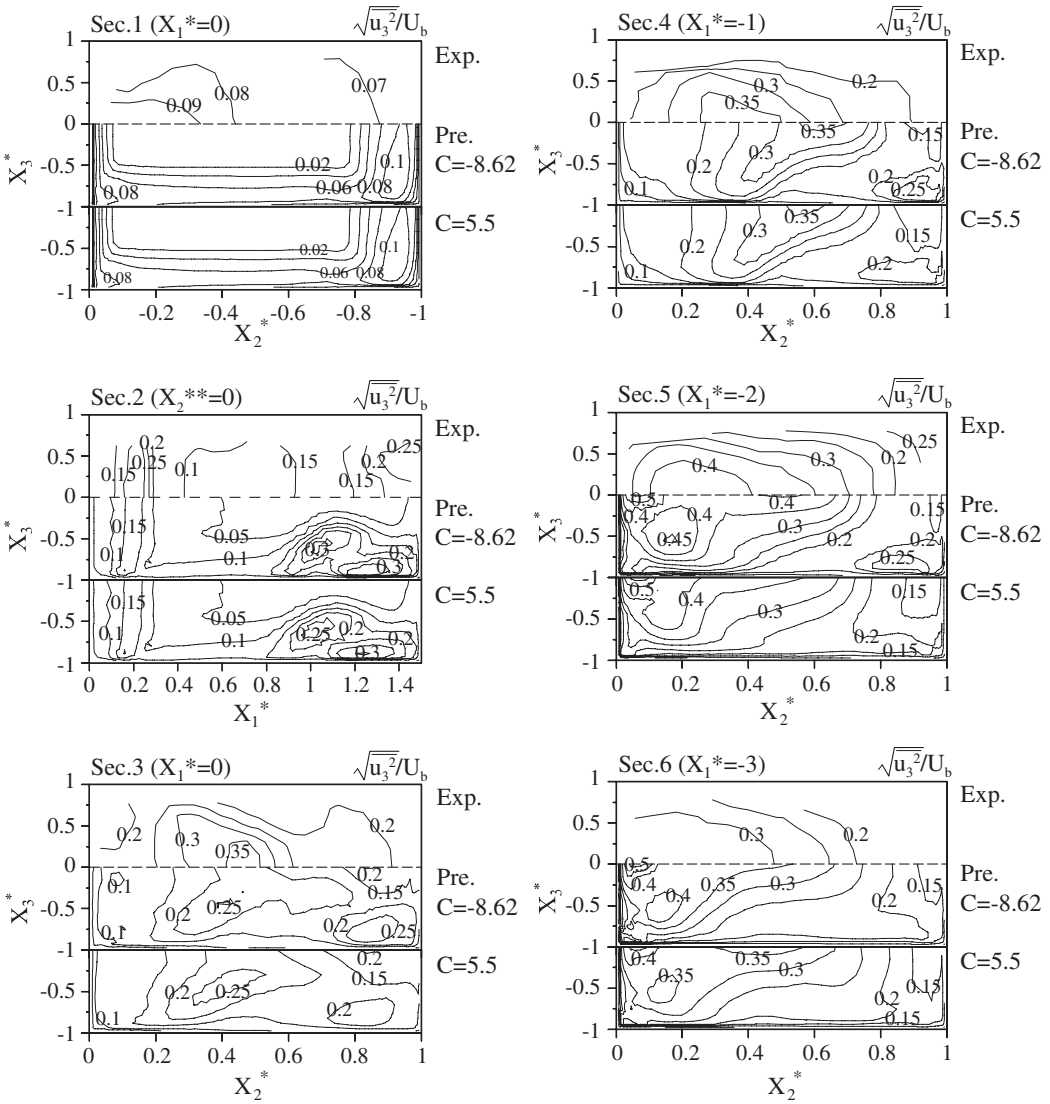

Figure 13. Comparison of vertically fluctuating velocity.

gradients $\partial U_2/\partial X_2$ and $\partial U_2/\partial X_3$. Considering that relatively high values are generated both near the wall and in the region located far from the wall in this rectangular duct with a sharp turn, the velocity gradient $\partial U_2/\partial X_1$ is thought to be important with respect to the generation of high values in the region far from the wall.

Figure 13 shows the comparison of the fluctuating velocity in the vertical direction parallel to the X_3^*-axis. Generally, the vertically fluctuating velocity is high along the vertical walls in the straight rectangular duct. The results calculated for Section 1 clearly have this characteristic feature, which is not always maintained through the entire flow and changes gradually as the flow develops. In the

DOI: 10.1002/fld

separated region, the high value near the inner and outer walls in Section 1 changes because of the separated flow, as shown in Section 2. In case of the calculation, the high value is generated more actively near the outer wall side, compared with the inner wall side. Based on the comparison results for Sections 3–5, a feature common to both the calculation and experimental results is that the maximum value is produced in the central region of the cross-section and the location of the maximum value moves toward the inner wall as the flow develops. Further downstream, in Section 6, the maximum value of the vertically fluctuating velocity for calculation appears on the inner wall side rather than on the outer wall side, which is the same for the stream-wise and horizontally fluctuating velocities. Considering the fact that Section 6 is located just after the reattachment point of the separated flow and the fluctuating velocity is generated actively near the reattachment point, the heat transfer is thought to be actively promoted after the reattachment point by the diffusion effect of fluctuating velocities.

Using the log-law velocity, two types of calculations have been performed for turbulent flow in a rectangular duct with sharp turns. One type of calculation involves the prediction of channel flow using the log-law velocity profile for smooth wall covering all the walls. The other type involves the adoption of the log-law velocity profile for roughened wall covering over only the separated region. The calculated results show that replacement of the log-law velocity over the separated region has a slight influence on the mean-velocity and fluctuating-velocity profiles. Although this replacement is not sufficient to accurately predict the experimental data, the proposed method has some potential for improving the prediction accuracy by changing the value of the universal constant of the log-law velocity.

5. CONCLUSIONS

A numerical analysis has been performed using an algebraic Reynolds stress model and a boundary-fitted coordinate system for a three-dimensional turbulent flow in a rectangular duct with a sharp 180-degree turn. This turbulent flow is characterized by the large-scale separated flow generated after the sharp turn. The calculated results are compared quantitatively with the experimental data measured by Nakayama *et al*. [8] to confirm the validity of the proposed method. Moreover, the application of the wall function method to the separated flow is examined by replacing the log-law velocity profile based on the flow conditions with and without a separated flow. The following conclusions are obtained based on the numerical analysis:

(1) Two types of calculations can be used to predict the experimental features of the main flow velocity. When the location of the zero-valued contour line of the main flow velocity is considered, both calculations reproduce the experimental contour lines, except for those of Section 5.
(2) Two types of calculations predict the reattachment point of the separated flow well. Comparison of the distribution of the stream function between the two types of calculation indicates that the method using the log-law velocity profile for a rough wall has some potential for improving the prediction accuracy by changing the value of the universal constant of the log-law velocity.
(3) Comparison of the experimental and calculated results for the secondary flow indicates a slight difference in the pair of vortices predicted near the reattachment point of the separated flow.

DOI: 10.1002/fld

(4) The proposed calculation enables the characteristic features of three types of velocity fluctuations to be reproduced but shows a tendency to underestimate the experimental value for almost all cross-sections.
(5) Based on comparison with the experimental data, the proposed algebraic Reynolds stress model can be used to predict a complicated turbulent flow with a separated flow.

NOMENCLATURE

D	long side of rectangular cross-section
D_h	hydraulic diameter
H	short side of rectangular cross-section
P	mean pressure
p	fluctuating pressure
P_k	production term of turbulent energy
k	turbulent energy
Re	Reynolds number $D_h U_b/v$
$\overline{u_i u_j}$	Reynolds stresses
U_b	bulk velocity
U_τ	friction velocity
U_i	velocity along the X_i-axis in rectangular coordinates
X_i	X_i-axis in rectangular coordinates
X_1^*	normalized axis X_1/D_h
X_2^{**}	middle location of the 180-degree curved duct
X_2^*	normalized axis X_2/D
X_3^*	normalized axis $X_3/(H/2)$
y	distance from the wall
t	time
δ_{ij}	Kronecker delta
ε	turbulent dissipation
v	kinematics viscosity
$\overline{(\ )}$	ensemble-averaged value

REFERENCES

1. Liou TM, Chen CC, Chen MY. Rotating effect on fluid flow in two smooth ducts connection by a 180-degree bend. *Journal of Fluids Engineering*, *Transactions of the ASME* 2003; **125**:138–148.
2. Apsley DD, Leschziner MA. Advanced turbulence modeling of separated flow in a diffuser. *Flow*, *Turbulence and Combustion* 1999; **63**:81–112.
3. Buice CU, Eaton JK. Experimental investigation of the flow through an asymmetric plane diffuser. *TSD-107, Department of Mechanical Engineering*, Stanford University, 1997.
4. Obi S, Aoki K, Masuda S. Experimental and computational study of turbulent separating flow in an asymmetric plane diffuser. *Ninth Symposium on Turbulent Shear Flows*, Kyoto, Japan, 1993; 305-1–305-4.
5. Hsieh SS, Chen PJ, Chin HJ. Turbulent flow in a rotating two pass smooth channel. *Journal of Fluids Engineering*, *Transactions of the ASME* 1999; **121**:725–734.
6. Iacovides H, Jackson DC, Kelemenis G, Launder BE, Yuan Y-M. LDA study of the flow development through an orthogonally rotating U-bend of strong curvature and rib roughened walls. *Engineering Turbulence Modelling and Experiments* 1996; **20**(3):561–570.

DOI: 10.1002/fld

7. Iacovides H, Jackson DC, Kelemenis G, Launder BE, Yuan Y-M. Flow and heat transfer in a rotating U-bend with 45° ribs. *International Journal of Heat and Fluid Flow* 2001; **22**:308–314.
8. Nakayama H, Hirota M, Fujita H, Yamada T, Koide Y. Flow characteristics in rectangular ducts with a sharp 180-degree turn. *Transactions of the JSME* 2003; **69-681**:1171–1179 (in Japanese).
9. Lin YL, Shih TIP, Stephens MA, Chyu MK. A numerical study of flow and heat transfer in a smooth and ribbed U-duct with and without rotation. *Journal of Heat Transfer*, *Transactions of the ASME* 2001; **123**:219–232.
10. Jang YL, Chen HC, Han JC. Computation of flow and heat transfer in two-pass channels with 60 deg ribs. *Journal of Heat Transfer*, *Transactions of the ASME* 2001; **123**:563–575.
11. Iacovides H, Raisee M. Recent progress in the computation of flow and heat transfer in internal cooling passages of turbine blades. *International Journal of Heat and Fluid Flow* 1999; **20**:320–328.
12. Sugiyama H, Watanabe C. Numerical analysis of developing turbulent flow in a U-bend of strong curvature with rib-roughened walls. *Transactions of the Atomic Energy Society of Japan* 2003; **2-1**:24–31 (in Japanese).
13. Sugiyama H, Watanabe C. Numerical analysis of developing turbulent flow in a rotating U-bend of strong curvature with rib-roughened walls. *Transactions of the Atomic Energy Society of Japan* 2003; **2-2**:24–31 (in Japanese).
14. Rodi W. A new algebraic relation for calculating the Reynolds stresses. *Zeitschrift fur Angewandte Mathematik and Mechanik* 1976; **56**:219–221.
15. Launder BE, Reece GJ, Rodi W. Progress in the development of a Reynolds stress turbulent closure. *Journal of Fluid Mechanics* 1975; **22**:537–566.
16. Gessner FB, Eppich HM. A near-wall pressure–strain model for turbulent corner flows. *Proceedings of the 3rd Symposium Turbulent Shear Flows*, The University of California, Davis, 1981; 25–32.
17. Sugiyama H, Hitomi D. Numerical analysis of developing turbulent flow in a 180° bend tube by an algebraic Reynolds stress model. *International Journal for Numerical Methods in Fluids* 2005; **47**:1431–1449.
18. Sugiyama H, Hitomi D, Saito T. Numerical analysis of turbulent structure in compound meandering open channel by an algebraic Reynolds stress model. *International Journal for Numerical Methods in Fluids* 2006; **51**:791–818.
19. Champangne FH, Harris VG, Corrsin S. Experimental on nearly homogeneous turbulent shear flow. *Journal of Fluid Mechanics* 1970; **41**:81–139.
20. Fujita H, Yokosawa H, Hirota H, Nishigaki S. Fully developed turbulent flow in a square duct with a rough wall. *Transactions of the JSME* 1987; **53-492**:2370–2376 (in Japanese).
21. Sugiyama H, Akiyama M, Nemoto Y, Gessner FB. Calculation of turbulent heat flux distributions in a square duct with one roughened wall by means of algebraic heat flux models. *International Journal of Heat and Fluid Flow* 2002; **23**:13–21.
22. Nakayama H, Hirota M, Ono Y, Fujita H. Flow characteristics in rectangular cross-sectioned two-pass channels with different channel aspect ratio. *Transactions of the JSME* 2005; **71-703**:781–788 (in Japanese).

DOI: 10.1002/fld